

SPECIAL SECTION - Brazilian Colloquiums on Geodetic Sciences



XII Colóquio Brasileiro
de Ciências
Geodésicas

V Simpósio
Brasileiro de
Geomática



Evaluation of OLI Landsat-8 images based on spectral indices in detecting areas affected by mining tailings mud: a case study of the Brumadinho dam rupture, Brazil

Beatriz Cirino Lucchetta¹ - ORCID: 0000-0002-7987-0927

Fernanda Sayuri Yoshino Watanabe² - ORCID: 0000-0002-8077-2865

Fernanda Silva Oliveira³

¹Post-Graduation Program in Cartography Sciences, School of Sciences and Technology, São Paulo State University (UNESP), Presidente Prudente, São Paulo State, Brazil.

E-mail: beatriz.lucchetta@unesp.br

² Department of Cartography, School of Sciences and Technology, São Paulo State University (UNESP), Presidente Prudente, São Paulo State, Brazil.

E-mail: fernanda.watanabe@unesp.br

³ Graduation in Environmental Engineering, School of Sciences and Technology, São Paulo State University (UNESP), Presidente Prudente, São Paulo State, Brazil.

E-mail: feeoliveira2808@gmail.com

Received in 03rd August 2023.

Accepted in 11th June 2024.

Abstract:

The socio-environmental impacts caused by the collapse of a mining dam can be irreversible. In Brazil, the dam collapse at the Córrego do Feijão Mine was considered one of the worst disasters in the country. Remote sensing-based approaches have been used to detect and monitor areas affected by tailings from dam rupture. Therefore, it was proposed to identify the area affected by mining tailing mud, in Brumadinho, Minas Gerais State, through the analysis of three different spectral indices: Normalized Difference Vegetation Index (NDVI), Ferrous Minerals Ratio (FMR) and Clay Minerals Ratio (CMR). These indices were computed from the Operational Land Imager (OLI) images of Landsat-8. Different thresholds were tested to define the best range for delineating the affected area. For validation, the limits of the affected area, obtained from a higher resolution sensor, GeoEye-1, were used as reference. The methodology demonstrated great potential for detecting areas affected by dam failure. The indices NDVI and FMR delimited the area of interest with high performance, with precision varying between 95% and 92%; recall between 88% and 87%; F-score between 91% and 89%; and global accuracy between 84% and 80%, showing to be suitable mapping such disasters.

Keywords: Environmental disasters; Multispectral images; Remote sensing; Geoprocessing; Iron ore; Córrego do Feijão Mine.

How to cite this article: LUCCHETTA BC, WATANABE FSY, OLIVEIRA FS. Evaluation of oli landsat-8 images based on spectral indices in detecting areas affected by mining tailings mud: a case study of the Brumadinho dam rupture, Brazil. *Bulletin of Geodetic Sciences*. 30: e2024013, 2024.



This content is licensed under a Creative Commons Attribution 4.0 International License.

1. Introduction

The iron ore extraction process consists of removing the ore from the rocks, using drills and detonators, and separating important material from material with no commercial value (Hk and Hossiney, 2022). Waste from the extraction of iron ore, composed of poor ores and water, is deposited in containment dams, in some cases using the waste itself as the bases, as it is contaminating and cannot be discarded in nature (Espósito, 2000).

When the dam exceeds its maximum containment capacity, there is a risk of a failure, which can cause disasters that are not bearable by nature or by the local communities (Polignano and Lemos, 2020). In Brazil, there were two major iron ore tailings dam collapses: the collapse of the Fundão dam in Mariana, in the State of Minas Gerais, controlled by Samarco Mineração S.A, in 2015, leaving 19 people dead; and the collapse of B1 dam (after called the Brumadinho dam) at the Córrego do Feijão Mine, in Brumadinho, also in Minas Gerais, controlled by Vale S.A company, in 2019, leaving 270 people dead. The Brumadinho dam collapse occurred on January 25th, 2019.

Dam failures associated with landslides and devastation of large areas are a global concern, as they can occur due to tectonic activities, climate variations or human actions. The social and physical damage generated can be irreversible (deaths and environmental destruction), in addition to the economic damage (Froud and Petley, 2018). Therefore, it is important to map vulnerable areas and regions where accidents have occurred to minimize damage, based on decision-making. Due to the environmental impacts of this type of disaster, several environmental monitoring studies, land use and land cover (LULC) analysis and contamination assessments of water bodies have been developed (e.g., Furlan et al., 2020, Rotta et al., 2020, Thompson et al., 2020, Pacheco et al., 2022, Mangussi Filho et al., 2023).

According Oliveira et al. (2009), the remote sensing is an important tool for environmental studies and, therefore, an alternative for mapping areas devastated by dam collapses. Recent works have approached different techniques for delimiting and monitoring areas affected by landslides and mining tailings. Studies related to the causes and environmental consequences of dam failures (Rotta et al., 2020), vulnerability analysis and risks of collapse of structures that store tailings (Mura et al., 2018, Du et al., 2020), landslides (Solari et al., 2020, Xu et al. 2023) and time series (Wasolki and Bovenga, 2014) were developed using an interferometric synthetic aperture radar (InSAR).

Other techniques that use different tools to extract or map devastated areas are, for example, pixel-based LULC classifications using Random Forest (Mangussi Filho et al., 2023), artificial neural networks and support vector machine (Syifa et al., 2019), as well as object-based image analysis (Hölbling et al., 2017). Landslides detection from multispectral images from different satellites has also been explored using machine learning techniques (Wang et al., 2023) and techniques based on shape-enhanced vision transformer model (Lv, et al., 2023). Foumelis (2017), on the other hand, used the normalized difference water index (NDWI) to delimit dam failure, in Larissa, Central Greece. The author compared multiples NDWI maps, developed from Sentinel-2 data as approach to detect the affected areas of road network.

In tragedies of large proportion such as Brumadinho dam collapse, it is expected that medium spatial resolution images and spectral enhancement algorithms, such as spectral indices, can delimit the area affected by the tailings mud. Thus, this study aimed to investigate the potential of three spectral indices in delimiting the area affected by tailings mud, in Brumadinho. Normalized Difference Vegetation Index (NDVI), Ferrous Minerals Ratio (FMR) and Clay Minerals Ratio (CMR) were calculated based on images from the Operational Land Imager (OLI) sensor, onboard the Landsat-8 satellite, with 30 m spatial resolution. Level-2 surface reflectance products, acquired on January 30th, 2019, were tested. The area and perimeter of the affected area were calculated based on the region enhanced by each spectral index. It was analyzed the spatial resolution suitability of the OLI sensor in delimiting the area of interest, comparing it with the delimitation derived by a high-resolution image. The combination of the use of remote sensing tools and geospatial analyses, in this case, guaranteed the delimitation of the tailings mud, which caused great destruction. This findings in this study can provide support for decision-making and public and environmental policies for the recovery, even in partial, of the affected area.

2. Methodology

2.1 Study area

The study area is located upstream of the city of Brumadinho, South-Central region of the State of Minas Gerais, Brazil, in a complex knowledge as “Quadrilátero Ferrífero”, where there are intense and predatory activities of iron ore extraction (Francisco, 2020). Activities at the Córrego do Feijão Mine began in 1941 and, in 2001, the company Vale do Rio Doce S.A. (currently Vale S.A.) took over management of the iron at the site (Milanez et al., 2019). With increase in the tailing deposit and exceeding the maximum capacity, the Córrego do Feijão Mine dam collapsed on January 25th, 2019. Approximately, 14 million tons of tailings spread about 10 km and reached the Paraopeba River (Rotta et al., 2020), an important affluent of São Francisco River and a water resource with multiple uses (Sato; Godinho, 2003). The area of interest (Figure 1(a)) is limited to the tailing’s accumulation area up to the Paraopeba River and is located between the coordinates $44^{\circ} 5' 45''$ W, $20^{\circ} 9' 54''$ S and $44^{\circ} 10' 8''$ O, $20^{\circ} 6' 52''$ S.

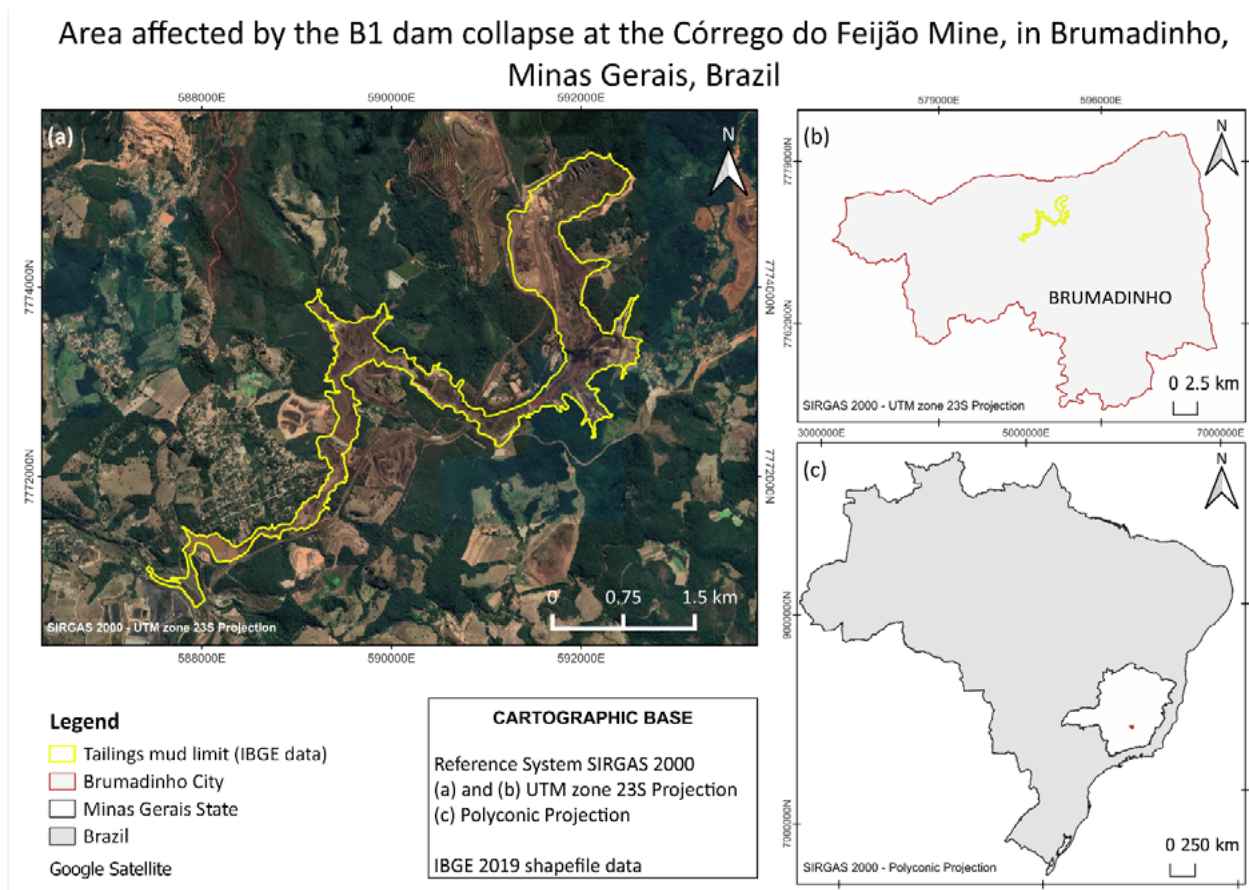


Figure 1: Study area map, where (a) is the area devastated by the tailings mud highlighted with a vector provided by IBGE, (b) is the location of the area of interest in the city of Brumadinho, and (c) is the location of the area of interest in the State of Minas Gerais and Brazil.

The Landsat image acquired on January 30th, 2019 shows the region affected by tailings mud. According to Rodrigues (2019), environmental damage can be irreversible, since mining waste devastated 133.27 ha of Atlantic Forest remnants, of which 71 ha were Permanent Preservation Areas (APPs), decimating all fauna and flora. The IBGE estimates an area around 297 ha covered by waste sludge (Villas Boas, 2022).

2.2 Image acquisition and processing

To detect the area affected by waste sludge, OLI images were downloaded free onto Earth Explorer platform, managed by the United States Geological Survey (USGS), via the website <https://earthexplorer.usgs.gov/>. Images acquired after the disaster, on January 30th, 2019 (5 days later), were used, corresponding path/row 218/074, which covers the entire area of interest. It is worth mentioning that the images are the product of surface reflectance (Collection 2 Level-2 processing), from the Land Surface Reflectance Code (LaSRC) algorithm (version 1.5.0), processed with Moderate Resolution Imaging Spectroradiometer - Climate Modeling Grid-Aerosol (MODIS CMA) as input data (Vermote et al., 2016), with no cloud cover over the study area. The OLI sensor contains nine spectral bands, with wavelengths ranging between 430 nm and 2290 nm. It is medium spatial resolution sensor, 30 m, and its revisit time is 16 days.

2.3 Spectral indices

The spectral indices were used to delimit the area of interest, as they allow specific targets to be highlighted on the Earth's surface, through the math operations of different spectral bands. In this study, three spectral indices were chosen due to their probable potential in highlighting tailings. Firstly, the Normalized Difference Vegetation Index (NDVI) was tested, because it is expected that it highlights the surrounding areas of the tailing mud, which are predominantly covered by vegetation. In addition to the vegetation index, two spectral indices were selected that highlight soil components, namely Ferrous Minerals Ratio (FMR) and Clay Minerals Ratio (CMR). FMR and CMR were tested because they enhanced iron minerals and hydrothermally altered rocks containing clay, respectively. Both materials made up the tailings mud.

NDVI is an index capable of highlighting areas that contain natural or secondary vegetation and agriculture, due the presence of chlorophyll or other photosynthetically active pigments. NDVI ranges from [-1; 1], where values close to one represent greater vegetative vigor, while values close to and less than zero show non-vegetated areas. Both FMR and CMR are band ratio whose results are greater than zero [0; ∞], where values closer to zero represent lower concentrations of minerals. The Red (R) (4), Near Infrared (NIR) (5), Shortwave Infrared 1 (SWIR 1) (6) and Shortwave Infrared 2 (SWIR 2) (7) bands were used to calculate the spectral indices: NDVI, FMR and CMR. The remote sensing analyses were performed in Quantum GIS (QGIS) freely available software, version 3.10.9.

NDVI was chosen to be used in this work, aiming to contrast areas where vegetation was devastated by tailings mud. The FMR may enhance areas with a high concentration of iron and, as the tailings are iron ore, the index is expected to perform well in highlighting the area of interest. In the same way as CMR, which aim to highlight areas with high concentrations of clay, a compound present in waste sludge, as well as silt. Table 1 shows the selected spectral indices.

Table 1: Equations of the spectral indices used to highlight the area affected by the tailings mud.

Index	Equation	Reference
NDVI	$\frac{NIR - R}{NIR + R}$	Rouse et al. (1973)
FMR	$\frac{SWIR 1}{NIR}$	Segal (1982)
CMR	$\frac{SWIR 1}{SWIR 2}$	Drury (1987)

2.4 Delimitation of the area of interest

The images resulting from the application of spectral indices were sliced using the Quantum GIS (QGIS) software, version 2.18, in order to delimit the region affected by the dam collapse. Slicing performs a one-dimensional classification of raster data, with the purpose of grouping pixels according to predetermined numerical ranges in a class (Reginaldo, 2015). For each index, different thresholds were experimentally tested, by trial and error, defining the maximum and minimum values, based on the analysis of the image histograms, which best delimit the area affected by the tailings mud.

The slicing tool separates pixels that have similar brightness values. Considering that other regions of the image could have the same pixel value as the area of interest, the raster data resulting from the slicing was converted into vector data and pixels not adjacent to the area of interest were excluded, to improve delimitation. From the best thresholds that defined the tailings mud area for each index, the area and perimeter of the vectors were calculated. To make the index results compatible with the IBGE vector (Paradella, 2019), it was necessary to adjust the Coordinate Reference System (CRS), once the IBGE vector data had been downloaded into SIRGAS 2000.

2.5 Validation

To evaluate the performance of the spectral indices in delimiting the area affected by tailing mud a vector data with the delimitation of the area of interest, provided by IBGE, was used. The IBGE vector data were generated from the vectorization of images from GeoEye-1 satellite, whose panchromatic band has 46 cm spatial resolution, while spectral band has 1.84 m. The GeoEye-1 used images taken on January 29th, 2019 (4 days after the disaster). These images make it possible to map the phenomena that occur in large areas on large cartographic scales (Paradella, 2019).

Since a binary classification was obtained, the evaluation metrics Precision (P), Recall (R), F-score and Global Accuracy (ACC) were used to assess the delimitation performance of each index. Precision is the ratio of the number of correctly classified pixels as tailings mud area (True Positive - TP) and the total number of pixels classified as area of interest (TP and False Positive - FP), as shown in Equation 1, i.e., relevant instances of each index. Recall is the ratio of the number of correctly classified pixels as tailings mud area (TP), and the total number of pixels that are tailings area (TP and False Negative - FN), as shown in Equation 2. F-score is a combination of Precision and Recall (Equation 3). Finally, Global Accuracy is the proportion of correctly classified pixels divided by the total number of pixels (Equation 4). The acronym FN represents false negatives.

$$P = \frac{TP}{TP + FP} \quad (1)$$

$$R = \frac{TP}{TP + FN} \quad (2)$$

$$F - score = \frac{2 \times P \times R}{P + R} \quad (3)$$

$$ACC = \frac{TP + TN}{TP + FP + TN + FN} \quad (4)$$

In addition to evaluating the metrics that measure the performance of the indices, the IBGE vector (Paradella, 2019) was taken as a reference and from it was subtracted the area and perimeter values calculated of the vectors coming to each index. Thus, there is a comparison between the vectors generated by the indices and the IBGE vector considered official.

3. Results

The results of the spectral indices applied in cropped images and their respective histograms are presented in Figure 2. Overall, the three indices highlighted the damaged area. As expected, NDVI highlighted the vegetation regions (brighter pixels) around the tailings mud area, consequently allowing to identify the area covered in mud, i.e., darker pixels. Unlike NDVI, the area of interest exhibited pixels in light gray shades for both FMR and CMR. By means of the histograms, it notes that the highest frequency peak does not cover the studied area, since there are more pixels exhibited outside the area of interest. The tailings mud area is highlighted in the histogram with a red line and arrow showing the appropriate range for local contrast of each index. Therefore, the intervals tested in the slicing tool were based on the histogram analysis and considering the minimum and maximum limit values of each index (NDVI with a range of [-0.64; 0.91], FMR with a range of [0.23; 2.23], CMR with a range of [0.32; 1.27]). Table 2 show the tested ranges.

Table 2: Four different ranges tested for each index: NDVI, FMR and CMR, in which one proved appropriate for the delimitation of tailings mud.

Tests	Ranges		
	NDVI	FMR	CMR
1	[-0.01; 0.3]	[0.5; 0.9]	[0.75; 1.5]
2	[0.01; 0.4]	[0.55; 0.8]	[0.95; 1.55]
3	[-0.22; 0.5]	[0.6; 0.95]	[0.95; 1.7]
4	[-0.02; 0.45]	[0.8; 1.0]	[0.95; 1.8]

*Check Table 1 for a better description of the selected indices.

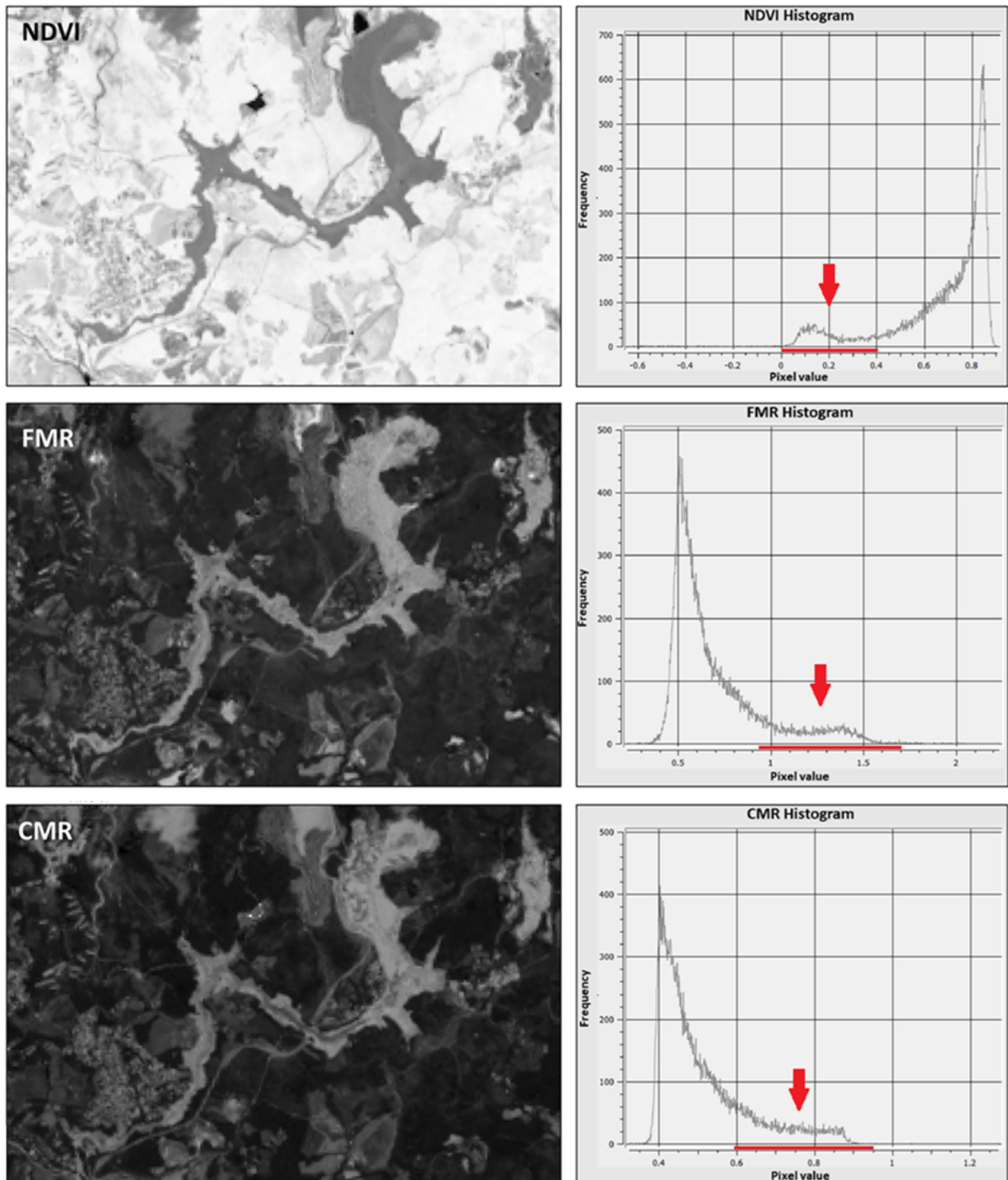


Figure 2: Images resulting from applying spectral indices NDVI, FMR and CMR, respectively, whose area of interest stands out in the center of the images taken on January 30, 2019. On the right side are the respective histograms of the images, in which the portion of the frequency that highlights the area of interest is evidenced with a red line and an arrow.

Among the different ranges tested, by trial and error, those that best defined the mud area were [0.01; 0.4] for NDVI, [0.95; 1.7] for FMR, and [0.6; 0.95] for the CMR. With the extraction of the tailings mud area by the range defined for each index, the raster data was converted into vector data and the pixels not adjacent to the devastated area were removed. The vectors referring to each index were generated and presented in Figure 3, jointly the area

and perimeter resulting from each index. It notes that the delimitations produced by NDVI (Figure 3(a)) and FMR (Figure 3(b)) are very similar to IBGE vector (Figure 3(d)).

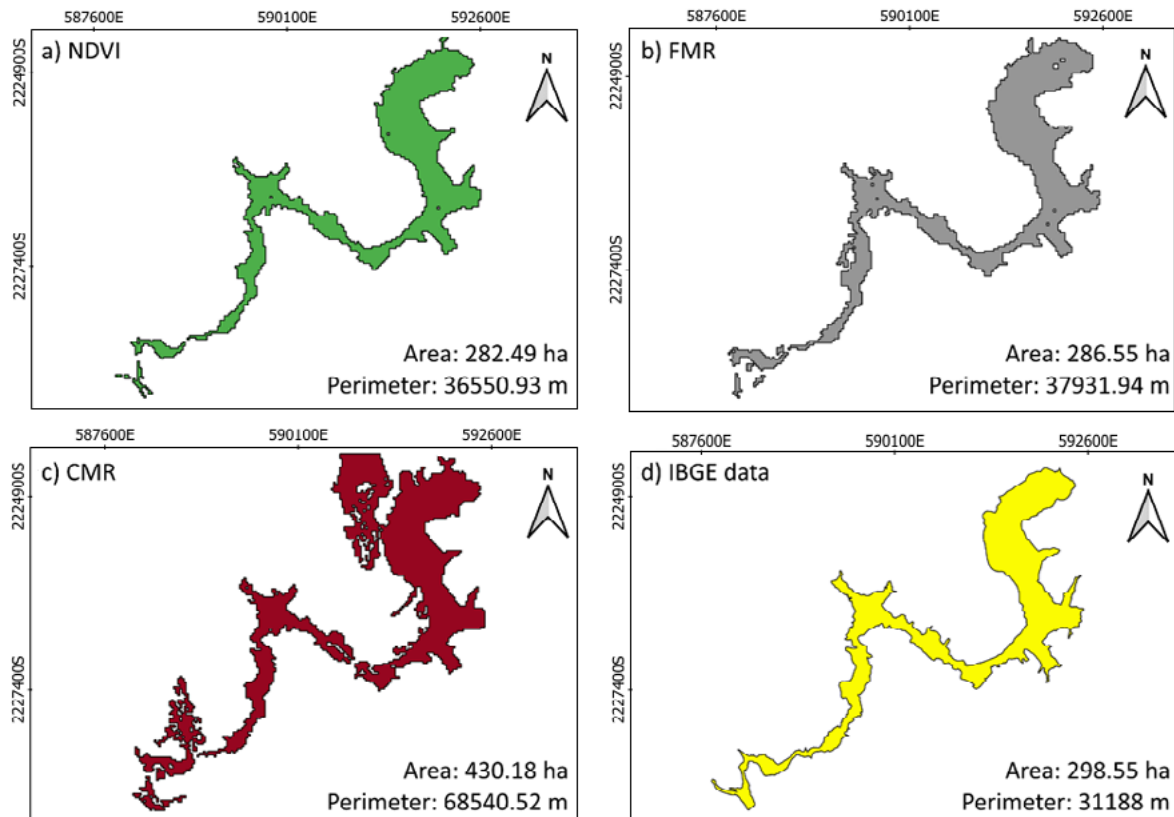


Figure 3: Result of the vectorization of the area affected by tailings sludge according to (a) NDVI, in green, (b) FMR, in gray, (c) CMR indices, in red, applied to the Landsat-8 image, and representation provided by (d) IBGE, in yellow. In each of the maps (a), (b), (c) and (d), the area and perimeter values for the respective vectors are calculated.

The IBGE vector has an area and perimeter of 298.55 ha and 31188 m, respectively. In relation to the areas of the calculated indices, the FMR resulted in a closer value to that derived from the IBGE vector, with a difference of 12 ha between them. The NDVI area did not result in a very different value, with a difference of around 16.06 ha. The perimeter of both indices also showed a small difference when compared to the IBGE vector, 6,743.34 m for FMR and 5,362.93 m for NDVI. Figure 4 shows the subtractions between the delimitations derived of the spectral indices and the data provided by IBGE.

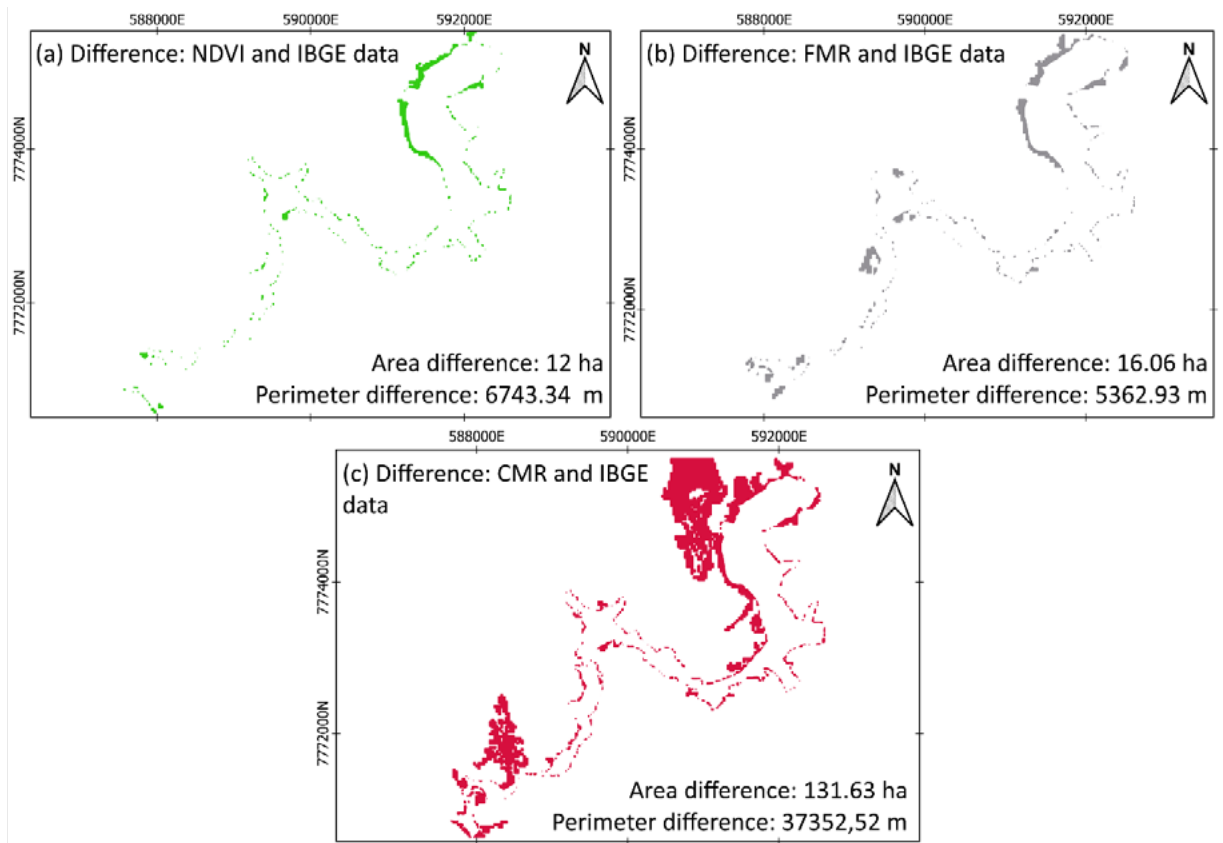


Figure 4: Result of the difference extracted between the vectors (a) NDVI and IBGE data, in green, (b) FMR and IBGE data, in gray, and (c) CMR and IBGE data, in red, and the difference between the area and perimeter values calculated between (a) NDVI and IBGE data, (b) FMR and IBGE data and (c) CMR and IBGE data.

On the other hand, the area and perimeter of CMR polygon did not approach the IBGE vector, with 430.18 ha and 68,540.52 m, respectively. These values are higher than those derived from its high-resolution images (Paradella, 2019), on the other side, CMR overestimated the areas affected by the disaster. There was a large occurrence of misclassified pixels, mainly caused by confusion with clouds that are in the upper left corner of the image, as well as confusion with an adjacent urban area. Furthermore, there was discontinuity in the affected area in several parts, due to false negatives, i.e., pixels that should have been classified as tailings mud.

Table 3 shows the performance of the spectral indices in defining the area of interest. In general, NDVI and FMR showed the best performance in defining the area damaged by tailings mud. All metrics exhibited results greater than 80% for both spectral indices. On the other hand, CMR did not have a good evaluation. As can be seen in Figure 4 (c) two areas adjacent to the tailings mud area were classified as area of interest. In other words, the high occurrence of FP decreases the CMR performance. Although recall metric was 93%, it is related to the number of FN pixels identified as area of interest, which in this case were few for this index, compared to the total number of pixels defined as tailings mud. In this type of classification, therefore, recall can mask the low performance of the classification.

Table 3: Performance evaluation metrics of spectral indices in the delimitation of the tailing's mud area.

Statistics	NDVI	FMR	CMR
Precision	95%	92%	65%
Recall	88%	87%	93%
Global Accuracy	84%	80%	62%
F-score	91%	89%	77%

4. Discussions

Besides the characteristics of the spectral indices, the differences among the delimitations generated in this study in relation to the IBGE vector may also be related to difference in spatial resolution between the Landsat-8 (30 m) and GeoEye-1 (0.5 m) images. Although the OLI sensor has a much lower spatial resolution than the GeoEye-1 sensor, the OLI images are considered suitable for this study, as the results produced were very close to those of the high spatial resolution sensor.

In a visual scope, the three spectral indices were able to delimit an area of interest, however the NDVI and FMR were more accurate than the CMR, due to the characteristics of the environmental surface that both indices are capable of highlighting. The CMR added part of an urban area (Bairro Parque da Cachoeira – Municipality of Brumadinho) as an area of interest, which can be seen in the lower left region of Figure 4(c). Urban areas have heterogeneous spectral characteristics (Small, 2005), i. e., there is a mix of built-up areas and other types of land cover, which favor the highlighting of the region by the applied index.

Additionally, a cloud and its shadow, which were not over the area but to the side, were highlighted by the CMR index. Clouds and their shadows are a problem for remote sensing, as they can hide important surfaces. The pixels identified in the upper region of Figure 4(c), adjacent to the dam collapse site, are the cloud and its shadow. These pixels were identified, since the cloud brightness is detected by the large magnitude spectral region of the visible, near-infrared and short-wave infrared (Zhai et al., 2018), which are spectral bands used to construct the index CMR (show Table 1).

The present work can be a reference for the use of other spectral indices, through a simple methodology, to highlight areas affected by mineral tailings or landslides, on low spatial resolution satellites, free available for the development of several futures works. For example, the following indices can be cited: Clay Alteration Index (CLAI) (Rowan and Mars, 2003); Ferric Iron Change Index (FEAI) (Mamouch et al., 2022); Laterite Index (LATI) (Guha et al., 2013); Silica Dioxide Index (SIDI) (Ninomiya, 2002); and others.

5. Conclusions

The main objective of delimiting the iron ore tailings mud, at Córrego do Feijão Mine, in Brumadinho, through the application of different spectral indices, was achieved. Among the indices tested, the NDVI and FMR showed the best performances in delimiting the area covered by the tailings mud, with accuracies greater than 80%, due to low presence of FPs and FNs. Furthermore, the image from the OLI sensor (30 m) showed satisfactory performance in delimiting the area of interest, despite the medium spatial resolution. Compared to the IBGE vector, NDVI and FMR showed similar delimitation.

In addition, although acquiring satellite images without cloud cover can be difficult in a rainy seasonal period,

such as is the austral summer in Brazil, when the date of the dam collapse occurrence, it was possible to acquire an image a few days after the event, without cloud cover over the area of interest. However, a cloud close to the area covered by the tailings mud harmed the CMR performance in delimiting the region affected by tailing mud, as the cloud pixels were highlighted as mud, generating FPs. Similarly, the urban area close to the area of interest also was enhanced as tailing mud by the CMR.

Finally, due to the importance of environmental monitoring of vulnerable areas or areas that have already suffered from environmental disasters such as dam collapses, other methodologies can be explored to delimit these locations. For future work it is recommended to use satellites with different spectral and spatial resolutions, e.g., Sentinel-2 MSI; application of other spectral indices; and more robust approaches, based on machine learning classifiers to delimit the area affected by tailings mud. Another option would be to test the panchromatic band of Landsat-8, due to the greater spatial resolution, and image fusion techniques to delimit the area of interest.

ACKNOWLEDGEMENT

The authors would like to thank the Post-Graduation Program in Cartographic Sciences from School of Sciences and Technology - FCT, São Paulo State University - UNESP, campus of Presidente Prudente/SP. Furthermore, the authors thanks São Paulo Research Foundation – FAPESP (Process N. 2021/11296-4), and Coordination of Superior Level Staff Improvement - CAPES for funding and research grants.

AUTHOR'S CONTRIBUTION

Lucchetta, B. C. contributed developing the study, experiments and results. Watanabe, F. S. Y. contributed with the supervision and methodological structuring. All authors written, revised and approved the final version of the manuscript.

REFERENCES

- Armstrong, M., Petter, R., Petter, C. 2019. Why have so many tailings dams failed in recent years?. *Resources Policy*, 63, p. 101412, 2019. DOI: 10.1016/j.resourpol.2019.101412.
- Drury, S. 1987. *Image Interpretation in Geology*. London: Allen and Unwin, 243 pp.
- Du, Z., Ge, L., Ng, A. H. M., Zhu, Q., Horgan, F. G., Zhang, Q. 2020. Risk assessment for tailings dams in Brumadinho of Brazil using InSAR time series approach. *Science of The Total Environment*, 717, 137125. DOI: 10.1016/j.scitotenv.2020.137125.
- Espósito, T. J. 2000. *Metodologia probabilística e observacional aplicada a barragens de rejeito construídas por aterro hidráulico*. PhD Teses - Universidade Federal de Brasília, Brasília, 363 p.
- Mangussi Filho, C. R., do Valle Junior, R. F., Silva, M. M. A. P., Mendes, R. G., Rolim, G. S, Pissarra, T. C. T., de Melo, M. C., Valera, C. A., Pacheco, F. A. L., Fernandes, L. F. S. 2023. The Accuracy of Land Use and Cover Mapping across Time in Environmental Disaster Zones: The Case of the B1 Tailings Dam Rupture in Brumadinho, Brazil. *Sustainability*, 15, 6949. DOI: 10.3390/su15086949.

- Foumelis, Michael. 2017. Impact of dam failure-induced flood on road network using combined remote sensing and geospatial approach. *Journal of Applied Remote Sensing*, 11.1, 016004-016004. DOI: 10.1117/1.JRS.11.016004
- Francisco, W. "Quadrilátero Ferrífero"; Brazil School. Available in: <<https://brasilecola.uol.com.br/geografia/quadrilatero-ferrifero.htm>>. Accessed on September 10th, 2020.
- Furlan, J. P. R., Santos, L. D. R., Moretto, J. A. S., Ramos, M. S., Gallo, I. F. L., Alves, G. D. A. D., Paulelli, A. C., Rocha, C. C. S., Cesila, C. A., Gallimberti, M., Devóz, P. P., Júnior, F. B., Stehling, E. G. 2020. Occurrence and abundance of clinically relevant antimicrobial resistance genes in environmental samples after the Brumadinho dam disaster, Brazil. *Science of The Total Environment*, 726, 138100. DOI: 10.1016/j.scitotenv.2020.138100.
- Guha, A., Singh, V. K., Parveen, R., Kumar, K. V., Jeyaseelan, A. T., & Rao, E. D. 2013. Analysis of ASTER data for mapping bauxite rich pockets within high altitude lateritic bauxite, Jharkhand, India. *International journal of applied earth observation and geoinformation*, 21, 184-194. DOI: 10.1016/j.jag.2012.08.003
- HK, T., Hossiney, N. 2022. A short review on environmental impacts and application of iron ore tailings in development of sustainable eco-friendly bricks. *Material Today: Proceedings*, 61, pp. 327-331. DOI: 10.1016/j.matpr.2021.09.522.
- Hölbling, D., Eisank, C., Albrecht, F., Vecchiotti, F., Friedl, B., Weinke, E., & Kociu, A. 2017. Comparing manual and semi-automated landslide mapping based on optical satellite images from different sensors. *Geosciences*, 7(2). DOI:10.3390/geosciences7020037.
- IBGE. Informações complementares para a região de Brumadinho – MG, 2019. Available in: <https://www.ibge.gov.br/np_download/novoportal/extras/Informacoes_complementaresBrumadinho_18fev2019.pdf>. Accessed on: November 23rd, 2020.
- Lv, P., Ma, L., Li, Q., Du, F. 2023. ShapeFormer: A Shape-Enhanced Vision Transformer Model for Optical Remote Sensing Image Landslide Detection. *IEEE Journal of Selected Topics in Applied Earth Observations and Remote Sensing*, 16, pp. 2681-2689. DOI: 10.1109/JSTARS.2023.3253769.
- Mamouch, Y., Attou, A., Miftah, A., Ouchchen, M., Dadi, B., Achkouch, L., Et-tayea, Y., Allaoui, A., Boualoul, M., Randazzo, G., Lanza, S., Muzirafuti, A. 2022. Mapping of hydrothermal alteration zones in the Kelâat M'Gouna region using airborne gamma-ray spectrometry and remote sensing data: mining implications (eastern anti-atlas, Morocco). *Applied Sciences*, 12, 957. DOI: 10.3390/app12030957.
- Milanez, B., Magno, L., Santos, R. S. P., Coelho, T. P., Giffoni Pinto, R., Wanderley, L. J. M., & Gonçalves, R. J. A. F. 2019. *Minas não há mais: avaliação dos aspectos econômicos e institucionais do desastre da Vale na bacia do rio Paraopeba*. Versos-Textos para Discussão PoEMAS, 3(1), pp. 1-114.
- Mura, J. C., Gama, F. F., Paradella, W. R., Negrão, P., Carneiro, S., Oliveira, C. G., & Brandão, W. S. 2018. Monitoring the vulnerability of the dam and dikes in Germano iron mining area after the collapse of the tailings dam of fundão (Mariana-MG, Brazil) using DInSAR techniques with terraSAR-X data. *Remote Sensing*, 10(10), 1507. DOI: 10.3390/rs10101507.
- Ninomiya, Y. 2002. Mapping quartz, carbonate minerals, and mafic-ultramafic rocks using remotely sensed multispectral thermal infrared ASTER data. In *Thermosense XXIV, SPIE*, 4710, 191-202. DOI: 10.1117/12.459566.
- Pacheco, F. A. L., Valle Junior, R. F., Melo, M. M. A. P., Pissarra, T. C. T., Melo, M. C., Valera, C. A., Fernandes, L. F. S. 2022. Prognosis of metal concentrations in sediments and water of Paraopeba River following the collapse of B1 tailings dam in Brumadinho (Minas Gerais, Brazil). *Science of The Total Environment*, 809, 151157. DOI: 10.1016/j.scitotenv.2021.151157.
- Paradella, R. Novos dados geoespaciais mostram área atingida pelo rompimento da barragem. Agência IBGE Notícias, Geociências, February 19th, 2019. Available in: <<https://agenciadenoticias.ibge.gov.br/agencia-noticias/2012-agencia-de-noticias/noticias/23808-novos-dados-geoespaciais-mostram-area-atingida-pelo-rompimento-da-barragem>>. Accessed on: March 28th, 2023.
- Polignano, M. V., Lemos R. S. 2020. Rompimento da barragem da Vale em Brumadinho: impactos socioambientais na Bacia do Rio Paraopeba. *Ciência e Cultura*, 72(2), pp. 37-43. DOI: 10.21800/2317-66602020000200011.

- Reginaldo, M. QGIS Python Plugins Repository. Available in: <<https://plugins.qgis.org/plugins/Slicer/>>. Accessed on: November 8th, 2020.
- Rodrigues, L. 2019. Ibama: tragédia de Brumadinho devastou 133 hectares de Mata Atlântica. Agência Brasil. Rio de Janeiro, 2019. Available in: <agenciabrasil.ebc.com.br/geral/noticia/2019-01/ibama-tragedia-de-brumadinhodevastou-133-hectares-de-mata-atlantica>. Accessed on: August 28th, 2020.
- Rotta, L. H., Alcântara, E., Park, E., Negri, R. G., Lin, Y. N., Bernardo, N., Mendes, T. S. G., Souza, C. R. 2020. The 2019 Brumadinho tailings dam collapse: Possible cause and impacts of the worst human and environmental disaster in Brazil. *International Journal of Applied Earth Observation and Geoinformation*, 90, 102109. DOI: 10.1016/j.jag.2020.102119.
- Rouse, J. W., Haas, R. H., Schell, J. A., Deering, D.W. 1973. Monitoring vegetation systems in the great plains with ERTS. In: Earth Resources Technology Satellite-1 Symposium. Proceedings. 3, pp. 309-317 In:Ponzoni, F. J., Shimabukuro, Y. E. *Sensoriamento remoto no estudo da vegetação*. p.144. São José dos Campos - SP: Editora Parêntese. Available in: <<http://www.cvmn.com.br>>. Accessed on: August 27th, 2020.
- Rowan, L. C., and Mars, J. C. 2003. Lithologic mapping in the Mountain Pass, California area using advanced spaceborne thermal emission and reflection radiometer (ASTER) data. *Remote sensing of Environment*, 84, 350-366. DOI: 10.1016/S0034-4257(02)00127-X.
- Sato, Y., Godinho, H.P. 2003. Migratory fishes of the São Francisco River. In: Carolsfeld, J., Harvey, B., Ross, C., Baer, A. (Eds.), *Migratory Fishes of South America*. World Fisheries Trust/The World Bank/International Development Research Centre, Ottawa, 195–232.
- Segal, D. 1982. Theoretical Basis for Differentiation of Ferric-Iron Bearing Minerals, Using Landsat MSS Data. *Proceedings of Symposium for Remote Sensing of Environment, 2nd Thematic Conference on Remote Sensing for Exploratory Geology*, Fort Worth, TX, pp. 949-951.
- Small, C. 2005. A global analysis of urban reflectance. *International Journal of Remote Sensing*, 26, 661 – 681. DOI: 10.1080/01431160310001654950.
- Syifa, M., Park, S.-J., Achmad, A.-R., Lee, C.-W., Eom, J. 2019. Flood mapping using remote sensing imagery and artificial intelligence techniques: A case study in Brumadinho, Brazil. In: Jung, H.-S., Lee, S., Ryu, J.H., and Cui, T. (eds.), *Advances in Remote Sensing and Geoscience Information Systems of Coastal Environments*. *Journal of Coastal Research*, Special Issue 90, pp. 197-204. DOI: 10.2112/SI90-024.1.
- Solari, L., Del Soldato, M., Raspini, F., Barra, A., Bianchini, S., Confuorto, P., Casagli, N., Crosetto, M. 2020. Review of Satellite Interferometry for Landslide Detection in Italy. *Remote Sensing*, 12, 1351. DOI: 10.3390/rs12081351.
- Thompson, F., Oliveira, B. C., Cordeiro, M. C., Masi, B. P., Rangel, T. P., Paz, P., Freitas, T., Lopes, G., Silva, B. S., Cabral, A. S., Soares, M., Lacerda, D., Vergilio, C. S., Lopes-Ferreira, M., Lima, C., Thompson, C., Rezende, C. E. 2020. Severe impacts of the Brumadinho dam failure (Minas Gerais, Brazil) on the water quality of the Paraopeba River. *Science of The Total Environment*, 705, 135914. DOI: 10.1016/j.scitotenv.2019.135914.
- United States Geological Survey (USGS). Disponível em: <<https://earthexplorer.usgs.gov/>>. Accessed on: August 28th, 2020. Sem autor: Science for a changing world.
- Vermote, E., Justice, C., Claverie, M., Franch, B. 2016. Preliminary analysis of the performance of the Landsat 8/OLI land surface reflectance product. *Remote Sensing of Environment*, 185, pp. 46-56. DOI: 10.1016/j.rse.2016.04.008.
- Villas Boas, B. Reflorestamento da área atingida pelo desastre de Brumadinho é 8% do que a Vale prometeu. Estadão, São Paulo, January 25th, 2022. Available in:<<https://www.estadao.com.br/brasil/reflorestamento-da-area-atingida-pelo-desastre-de-brumadinho-e-8-do-que-vale-prometeu/>>. Accessed on: March 28th, 2023.
- Wang, J., Chen, G., Jaboyedoff, M., Derron, M. H., Fei, L., Li, H., Luo, X. 2023. Loess landslides detection via a partially supervised learning and improved Mask-RCNN with multi-source remote sensing data. *Catena*, 231, 107371. DOI: 10.1016/j.catena.2023.107371.

Wasowski, J., Bovenga, F. 2014. Investigating landslides and unstable slopes with satellite Multi Temporal Interferometry: Current issues and future perspectives. *Engineering Geology*, 174, 103-138. DOI: 10.1016/j.enggeo.2014.03.003.

Xu, Q., Zhao, B., Dai, K., Dong, X., Li, W., Zhu, X., Yang, Y., Xiao, X., Wang, X., Huang, J., Lu, H., Deng, B., Ge, D. 2023. Remote sensing for landslide investigations: A progress report from China. *Engineering Geology*, 321, 107156. DOI: 10.1016/j.enggeo.2023.107156.

Zhai, H., Zhang, H., Zhang, L., Li, P. 2018. Cloud/shadow detection based on spectral indices for multi/hyperspectral optical remote sensing imagery. *ISPRS Journal of Photogrammetry and Remote Sensing*. 144, 235 – 253. DOI: 10.1016/j.isprsjprs.2018.07.006.